Dynamical Decoupling of Nitrogen-Vacancy Electron Spins in Diamond and Nanodiamond

Richard Kullmann

26. Februar 2018

Motivation

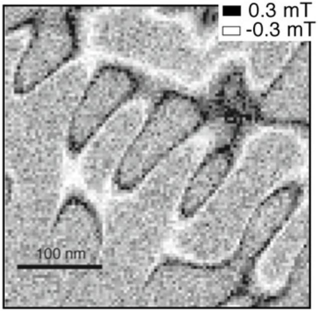

magnetic imaging of a hard disk using NV centers, taken from [1]

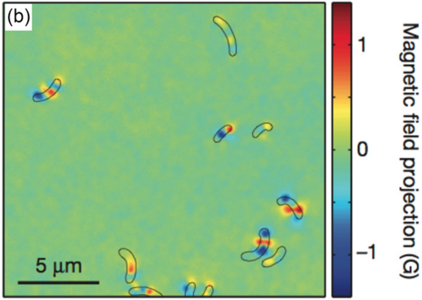

wide-field image of magnetotactic bacteria, obtained with NV magnetometer, taken from [1]

[1] L. Rondin et al., "Magnetometry with nitrogen-vacancy defects in diamond," *Rep. Prog. Phys. 77*, 2014.

Motivation

- magnetometry: usage of single spins as quantum sensors
- sensitivity [1]:

$$\eta = \frac{\pi\hbar}{2g\mu_B C\sqrt{N\cdot T_2}}$$

$\rightarrow$ large T_2 time necessary for good resolution

- T_2 affected by interactions with surrounding spins
- **Dynamical decoupling sequences**

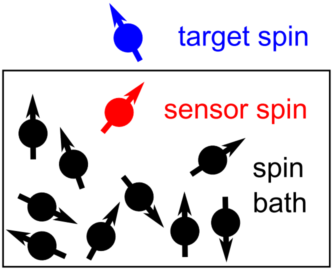

sensor spin in magnetic environment

[1] L. M. Pham, *Magnetic Field Sensing with Nitrogen-Vacancy Color Centers in Diamond*. PhD thesis, The School of Engineering and Applied Sciences, 2013.

NV center

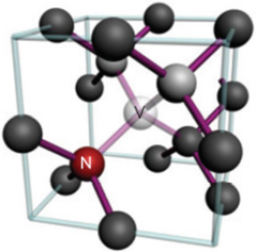

structure of an NV center, taken from [1]

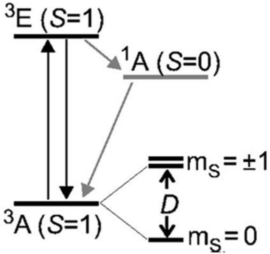

NV energy level scheme, taken from [2]

- $m_s = 0$ and $m_s = \pm 1$ sublevels separated by D=2.87GHz
- fluorescence with ZPL at 637 nm
- $m_s = 0$: bright state, $m_s = \pm 1$: dark state

[1] L. Rondin et al., "Magnetometry with nitrogen-vacancy defects in diamond," *Rep. Prog. Phys. 77*, 2014.

[2] R. Hanson et al., "Room-temperature manipulation and decoherence of a single spin in diamond," *Physical Review B 74*, 2006.

Rabi oscillations

- two level system with AC magnetic field
- Rabi's formula for resonant excitation:

$$P_{1\to 0}(t) = \sin^2\left(\frac{\omega_1 t}{2}\right)$$

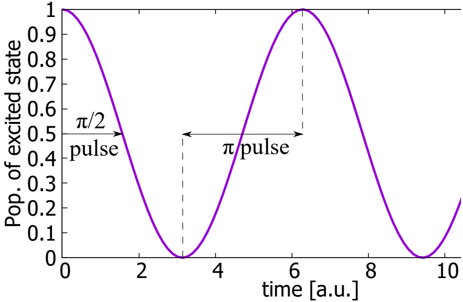

Rabi oscillations under resonant excitation

↷ **π and $\pi/2$ pulses**

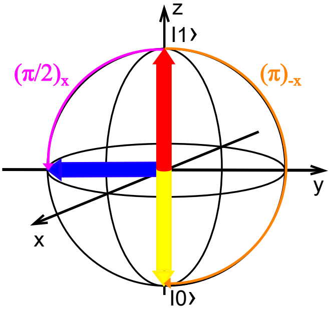

rotations on the Bloch sphere

Dynamical decoupling sequences

Hahn Echo

- cancels slowly varying inhomogeneities

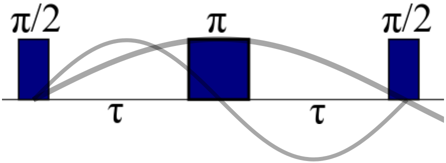

CPMG

- single axis rotations
- higher decoupling efficiency than Hahn Echo

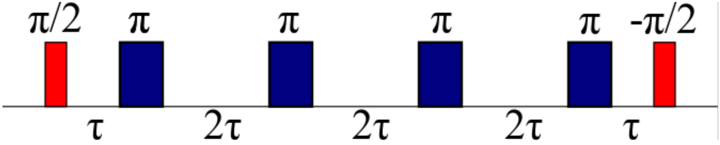

CPMG-4 pulse sequence

Dynamical decoupling sequences

XY

- CPMG pulse spacing
- alternating π_x and π_y pulses perform 3D decoupling

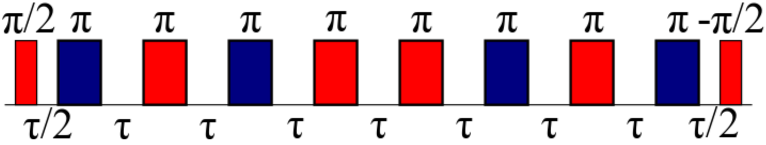

XY-8 sequence: red pulses are π_y and blue pulses are π_x

UDD

- no equidistant spacings

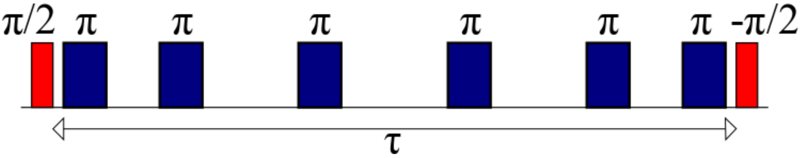

UDD-6 sequence

Setup

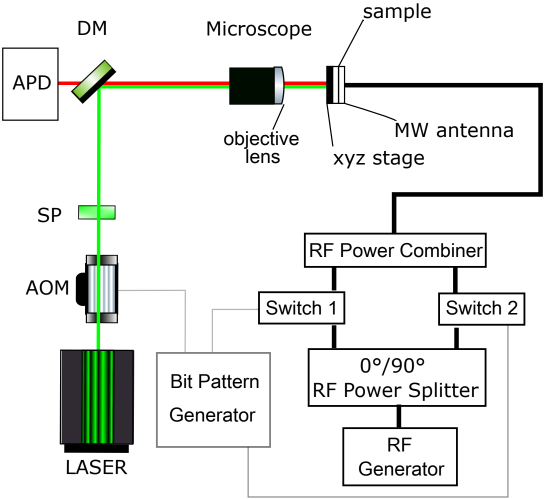
sample
DM
Microscope
APD
objective lens
MW antenna
xyz stage
SP
AOM
RF Power Combiner
Switch 1
Switch 2
0°/90°
RF Power Splitter
Bit Pattern Generator
RF Generator
LASER

Resonance scan and Hahn Echo

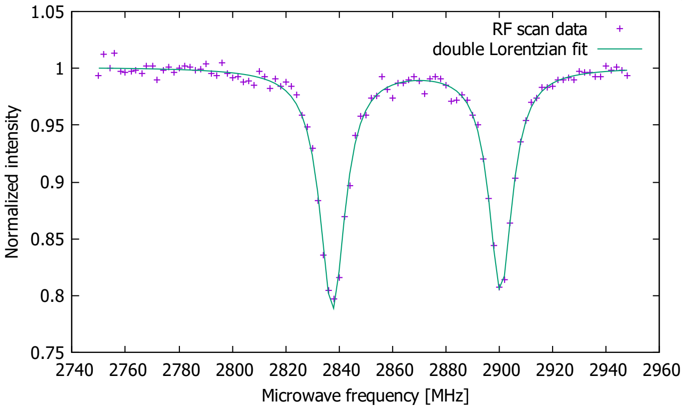

Resonance scan and Hahn Echo

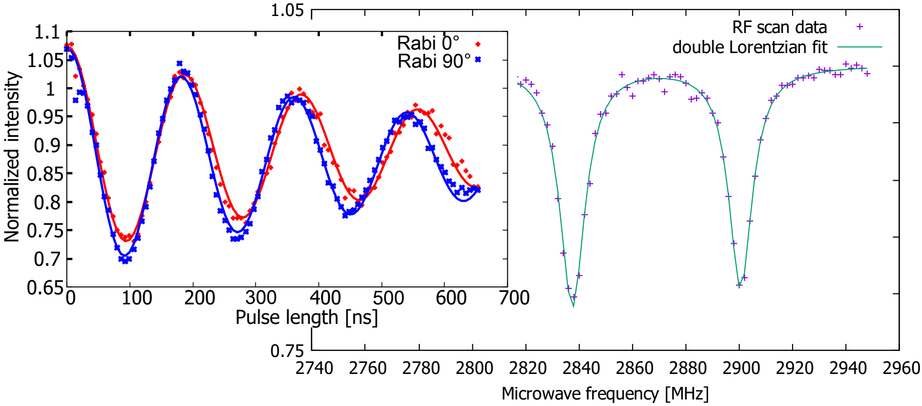

Resonance scan and Hahn Echo

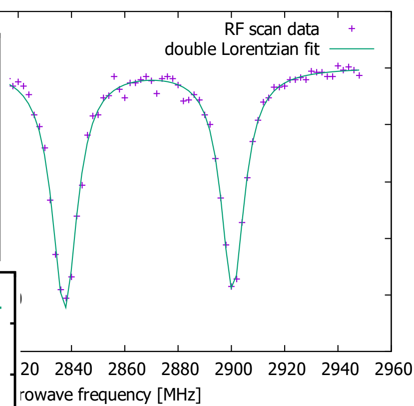

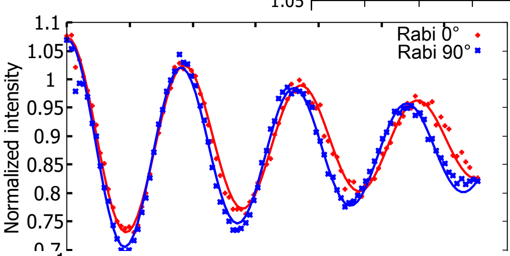

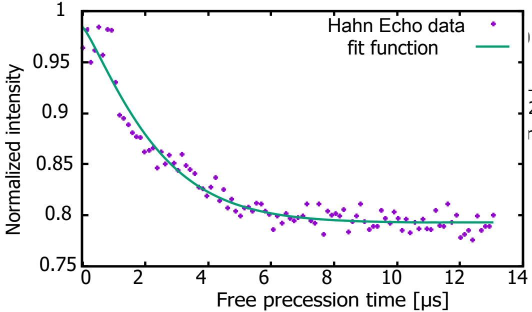

$$\boxed{T_{2,H} = (2.41 \pm 0.12)\mu s}$$

CPMG

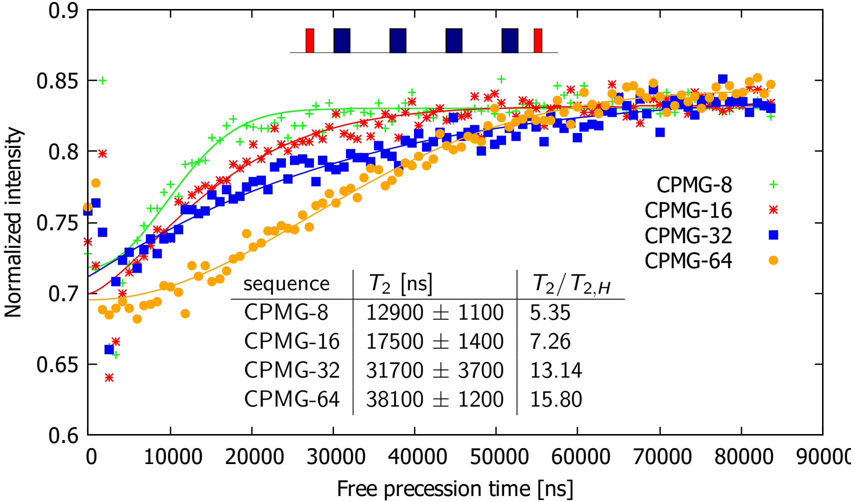

sequence	T_2 [ns]	$T_2/T_{2,H}$
CPMG-8	12900 ± 1100	5.35
CPMG-16	17500 ± 1400	7.26
CPMG-32	31700 ± 3700	13.14
CPMG-64	38100 ± 1200	15.80

Comparison of CPMG-sequences with different numbers of pulses

XY

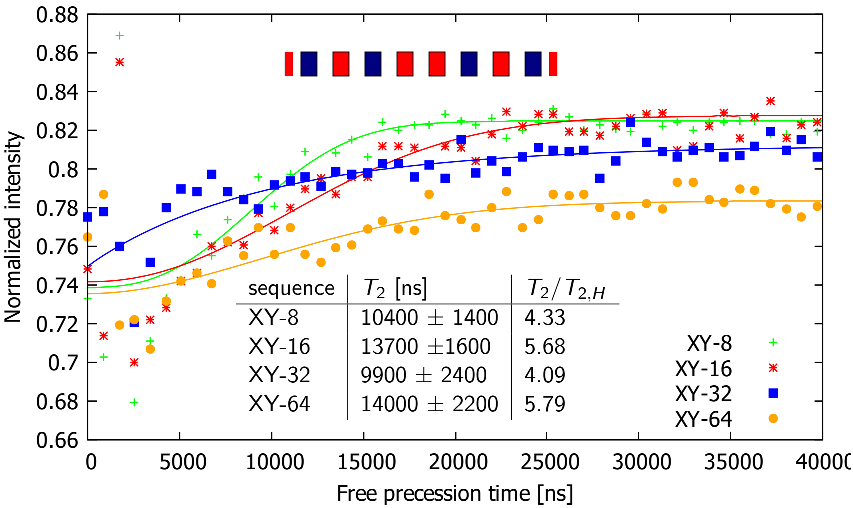

sequence	T_2 [ns]	$T_2/T_{2,H}$
XY-8	10400 ± 1400	4.33
XY-16	13700 ± 1600	5.68
XY-32	9900 ± 2400	4.09
XY-64	14000 ± 2200	5.79

Comparison of XY-sequences with different numbers of pulses

UDD

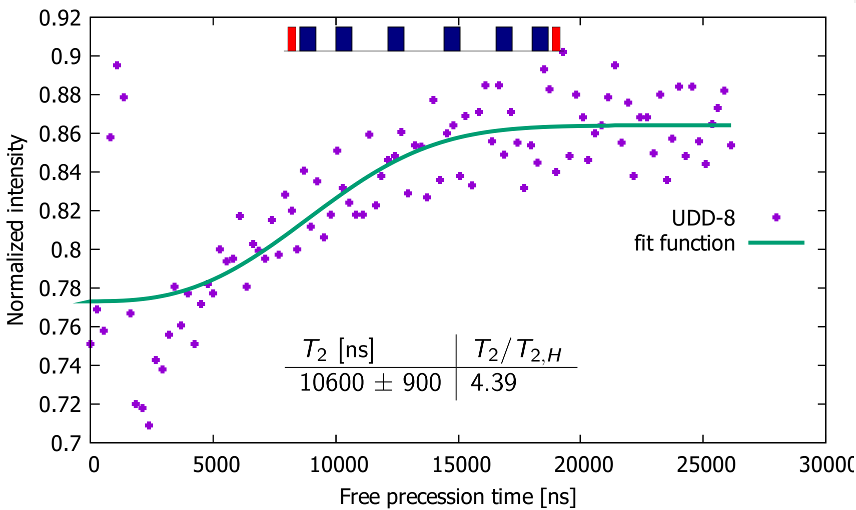

Performance of UDD on nanodiamond

Different NVs

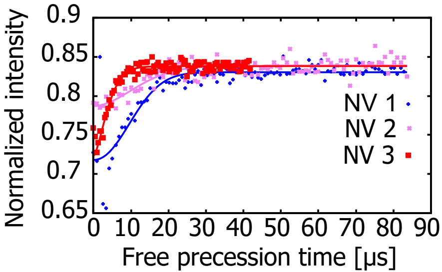

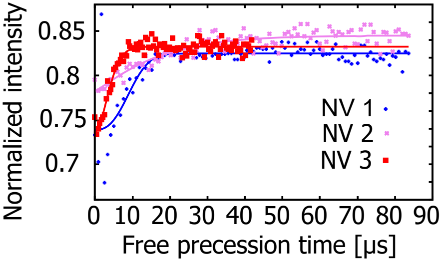

CPMG-8 for different NVs

	T_2 [ns]	$T_2/T_{2,H}$
NV 1	12900 ± 1100	5.35
NV 2	5000 ± 200	3.45
NV 3	14700 ± 1400	16.63

XY-8 for different NVs

	T_2 [ns]	$T_2/T_{2,H}$
NV 1	10700 ± 1000	4.42
NV 2	4600 ± 200	3.18
NV 3	17000 ± 2000	19.42

Comparison of XY and CPMG

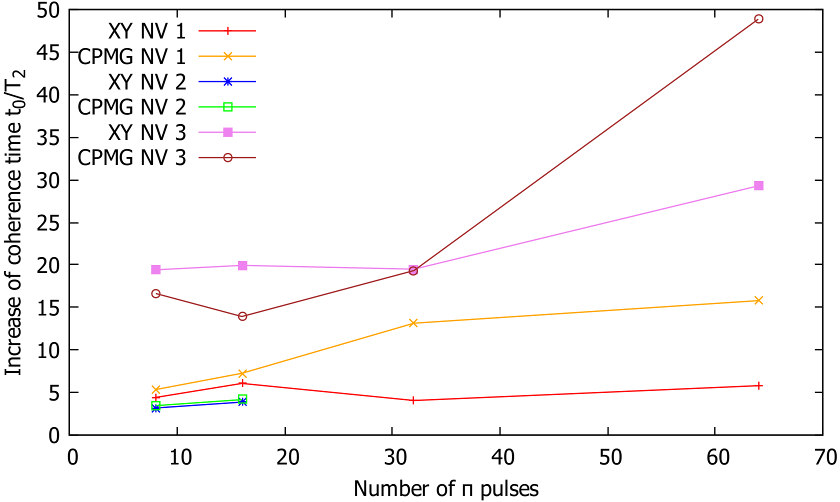

performance of XY and CPMG on nanodiamonds

Dynamical decoupling sequences

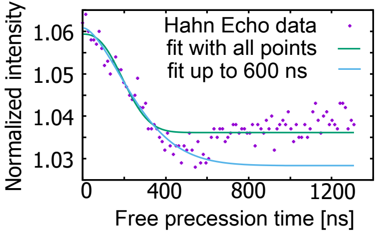

Hahn Echo: $T_2(t \leq 600\text{ns}) = (302 \pm 25)\text{ns}$

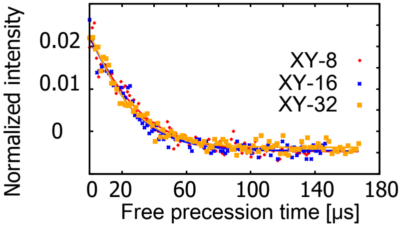

XY on the bulk diamond

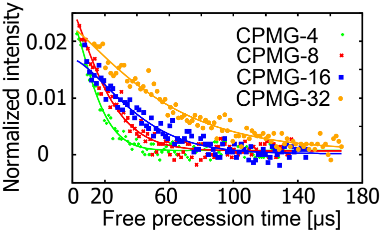

CPMG on the bulk diamond

- T_2 improvement up to factor 200 for CPMG
- T_2 increased by factor of about 90 for all XY
- CPMG outperforms XY

Spectral decomposition

- loss of coherence can be described using

$$C(t) = e^{-\chi(t)}$$

with[1]

$$\chi(t) = \frac{1}{\pi}\int_0^\infty d\omega S(\omega)\frac{F(\omega t)}{\omega^2}$$

$F(\omega t)$ filter function, $S(\omega)$ spectral density function

- $S(\omega)$ assumed to have Lorentzian shape[1]:

$$S(\omega) = \frac{\Delta^2\tau_c}{\pi}\frac{1}{1+(\omega\tau_c)^2}$$

Δ average coupling strength of spin bath to the probed NVs,
τ_c correlation time of N bath spins with each other

[1] N. Bar-Gill et al., "Suppression of spin-bath dynamics for improved coherence of multi-spin-qubit systems," *Nature Communications 3, Article number: 858*, 2012.

Spectral decomposition

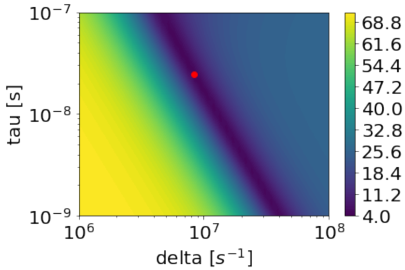

calculation for CPMG-32

- correlation between Δ and τ_c
- for $\omega \ll \tau_c^{-1}$:

$$S(\omega) = \frac{\Delta^2 \tau_c}{\pi}$$

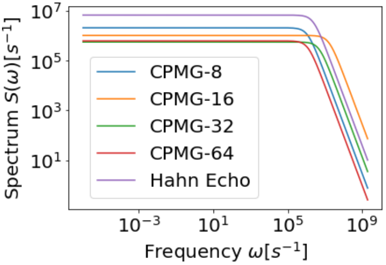

spectral densities for all sequences

sequence	τ_c[ns]	Δ[MHz]
Hahn	66	18
CPMG-8	89	8
CPMG-16	10	18
CPMG-32	32	7
CPMG-64	125	4

Spectral decomposition

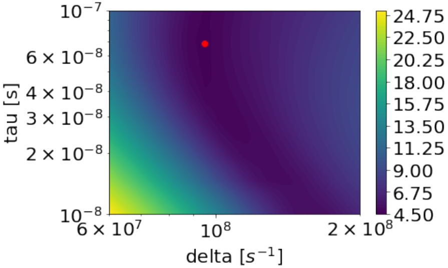

calculation for Hahn

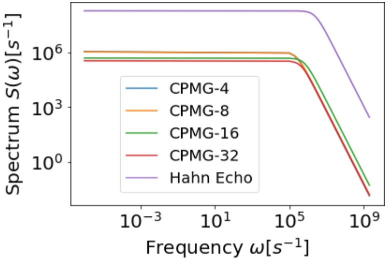

spectral densities for all sequences

- same correlation as before
- similar experiments[1] : $1\text{MHz} \leq \Delta \leq 10\text{MHz}$ and $1\mu\text{s} \leq \tau_c \leq 15\mu\text{s}$

sequence	τ_c[ns]	Δ[MHz]
Hahn	69	95
CPMG-4	700	2.2
CPMG-8	650	2.3
CPMG-16	250	2.5
CPMG-32	370	1.7

[1] N. Bar-Gill et al., "Suppression of spin-bath dynamics for improved coherence of multi-spin-qubit systems," *Nature Communications 3, Article number: 858*, 2012.

Conclusion and Outlook

- successful implementation of DD protocols
- CPMG outperforms XY
- improvement of factor 50 in nanodiamond and 200 in bulk diamond $\rightarrow T_2 = 50\mu\text{s}$
- spectral density analysis provided information about the surrounding magnetic environment
- sensitivity:

$$\eta = \frac{\pi\hbar}{2g\mu_B C\sqrt{N \cdot T_2}}$$

$\rightarrow \eta_{ND} \approx 10\text{nT}/\sqrt{Hz}$, $\eta_{BD} \approx (6\text{-}18)\text{nT}/\sqrt{Hz}$

- error sources: BPG (pulse errors), MW splitter, AOM
- future:
  - better time and phase control
  - implementation of other decoupling protocols